inorganics

MDPI

Article

Iridium(III) and Rhodium(III) Half-Sandwich Coordination Compounds with 11*H*-Indeno[1,2-b]quinoxalin-11-one Oxime: A Case of Spontaneous Resolution of Rh(III) Complex

Vladislava V. Matveevskaya, Dmitry I. Pavlov and Andrei S. Potapov *

Nikolaev Institute of Inorganic Chemistry, 3 Lavrentiev Ave., 630090 Novosibirsk, Russia
* Correspondence: potapov@niic.nsc.ru; Tel.: +7-(383)-330-92-56

Abstract: Two half-sandwich iridium(III) and rhodium(III) complexes with 11*H*-indeno[1,2-b]quinoxalin-11-one oxime (IQ-1) ligand were prepared by the reaction of the proligand with $[M(Cp^*)Cl_2]_2$ (M = Ir, Rh) dimers. The reaction between IQ-1 and $[Ir(Cp^*)Cl_2]_2$ in methanol gave the complex [Ir(Cp*)(IQ-1)Cl] (**1**), which crystallized in a centrosymmetric space group as a true racemate. Whereas complex [Rh(Cp*)(IQ-1)Cl] (**2**) in the form of a racemic conglomerate was obtained by the reaction of $[Rh(Cp^*)Cl_2]_2$ and IQ-1 in methanol. The crystal structures of complexes **1** and **2** (*R* and *S* enantiomers) were determined by X-ray diffraction analysis, and the structural features were compared in order to understand the structural factors leading to the spontaneous enantiomer resolution of the rhodium(III) complex. In the crystal packing of **1**, intermolecular C–H···C contacts between a pair of enantiomers link the molecules into centrosymmetric dimers and lead to the formation of heterochiral crystals of **1**. In contrast, the intramolecular contacts CH···Cl and CH···C in complex **2** bind all three ligands around the chiral Rh(III) metal center. In addition, a combination of intermolecular CH···O and CH···C contacts leads to the formation of a homochiral supramolecular structure. These interactions altogether reinforce the spontaneous resolution in complex **2**.

Keywords: iridium; rhodium; 11*H*-indeno[1,2-b]quinoxalin-11-one oxime; IQ-1; chirality; spontaneous resolution; achiral precursors; racemic conglomerate

Citation: Matveevskaya, V.V.; Pavlov, D.I.; Potapov, A.S. Iridium(III) and Rhodium(III) Half-Sandwich Coordination Compounds with 11*H*-Indeno[1,2-b]quinoxalin-11-one Oxime: A Case of Spontaneous Resolution of Rh(III) Complex. *Inorganics* **2022**, *10*, 179. https://doi.org/10.3390/inorganics10110179

Academic Editor: László Kótai

Received: 30 September 2022
Accepted: 24 October 2022
Published: 25 October 2022

1. Introduction

Recently, iridium(III) and rhodium(III) complexes have gained a lot of attention as luminescent agents [1–4], chemo- and biosensors [5–8], biologically active compounds [9–12], and especially as catalysts [13–15]. Chiral half-sandwich Cp*Ir and Cp*Rh complexes were successfully applied in asymmetric catalysis, most importantly, the catalytic activation of C–H bonds [16–19]. The general approach to the synthesis of chiral coordination compounds consists of using enantiopure ligands to obtain complexes of the same absolute configuration [20]. Another approach is exploiting the chirality of the metal center, which can be induced by the chiral agent to form enantiopure complexes [21]. Both ways require homochiral compounds (ligands, catalyst, solvent, or chiral inducer that does not directly participate in the reaction). However, because of the high cost of homochiral compounds and the possibility of their racemization during the reactions, the synthesis of enantiopure complexes from achiral or racemic precursors without any chiral condition is a great challenge. Thereby, the spontaneous resolution upon crystallization of achiral precursors has the potential to advance as an effective method. The asymmetric arrangement of ligands around a metal center through non-covalent interactions is a key factor in the spontaneous resolution. Racemic conglomerates contain equal amounts of left- and right-handed crystals, but individual crystals are homochiral and in some cases can be separated manually. However, the spontaneous resolution process remains, to a great extent, unpredictable and examples of Ir(III) and Rh(III) racemic conglomerates are rare [22–25].

Recently, we published a series of half-sandwich Ru(II) complexes containing 11*H*-indeno[1,2-b]quinoxalin-11-one oxime (**IQ-1**, Scheme 1) derivatives, which exhibited biological and catalytic properties [26,27]. All complexes had chiral ruthenium(II) centers but crystallized in centrosymmetric space groups and thus enantiomer resolution was not possible. Polycyclic **IQ-1** derivatives look promising as ligands in terms of stabilizing the complexes due to π–π stacking interactions and their biological properties [28–31]. In the present paper, the **IQ-1** ligand was used to prepare new half-sandwich cyclopentadiene iridium(III) and rhodium(III) complexes, and for the rhodium(III) coordination compound, a spontaneous resolution of enantiomers was observed.

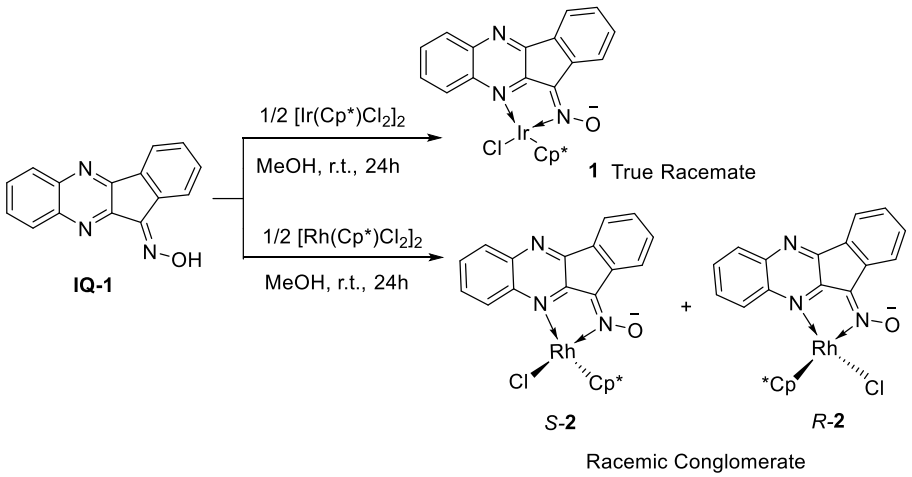

Scheme 1. Synthesis of coordination compounds **1** and **2**.

2. Results and Discussion

2.1. Synthesis of Coordination Compounds

Iridium(III) and rhodium(III) coordination compounds [Ir(Cp*)(**IQ-1**)Cl] (**1**) and [Rh(Cp*)(**IQ-1**)Cl] (**2**) were prepared by the reaction of the oxime **IQ-1** (1 equiv.) and pentamethylcyclopendiene (Cp*) dimers $[M(Cp^*)Cl_2]_2$ (M = Ir^{3+}, Rh^{3+}, 0.5 equiv.) in methanol at room temperature (Scheme 1). The products initially precipitated as powders and single crystals were obtained upon cooling the filtrate.

The compounds were characterized by elemental analysis, IR and NMR spectroscopy as well as single-crystal X-ray diffraction (SC-XRD) analysis, which revealed that both compounds had the chemical formula [M(Cp*)(**IQ-1**)Cl] (M = Ir (**1**) and Rh (**2**)).

Single crystals of compounds **1** and **2**, suitable for SC-XRD analysis were obtained by cooling the filtrates of the reaction mixtures at 4 °C. Interestingly, the Ir(III) complex **1** crystallized in a centrosymmetric space group as a true racemate, whereas the Rh(III) complex **2** formed a racemic conglomerate of *S*-**2** and *R*-**2** crystals.

Powder X-ray diffraction (PXRD) analysis was used to evaluate the phase composition of the obtained powder and crystalline products. For compound **1**, PXRD patterns of both the initial powder precipitate and the crystals formed from the filtrate corresponded very well to the pattern calculated from the SC-XRD data (Figure S1), confirming the phase homogeneity of the formed product. For compound **2**, PXRD pattern for the crystalline product was in accordance with the SC-XRD analysis, while several additional peaks were present in the pattern of the powder product (Figure S2), probably as a result of some amount of a centrosymmetric phase. Thus, in the case of compound **2**, only the crystalline product was used for further studies.

2.2. Spectroscopic Characterization

IR spectra of the complexes provide evidence for the coordination mode of the **IQ-1** ligand in compounds **1** and **2** (Figures S3 and S4). The free oxime ligand exhibits a broad band at 3200–3250 cm^{-1}, corresponding to O–H stretching vibrations in the oxime func-

tional group and a band of oxime C=N stretching vibration near 1646 cm^{-1} [32]. In the IR spectra of the complexes, the former band was not detected, while the latter was shifted toward a lower frequency for compound **1** (1610 cm^{-1}) and not changed for compound **2** (1647 cm^{-1}), confirming the coordination of oxime **IQ-1** in an anionic form. The bending vibration bands of the methyl groups in the Cp* ligand were observed at 1479 cm^{-1} (**1**) and 1490 cm^{-1} (**2**) with a slight shift to the higher frequency compared to the $[Ir(Cp^*)Cl_2]_2$ (1452 cm^{-1}) and $[Rh(Cp^*)Cl_2]_2$ (1476 cm^{-1}) dimers. The bands of the Cp* ring vibrations in complex **1** (968 cm^{-1}) and **2** (1001 cm^{-1}) shifted to a lower frequency relative to the Ir (1033 cm^{-1}) and Rh (1028 cm^{-1}) precursors.

The coordination mode of the **IQ-1** ligand and the formation of a mono-nuclear complex was also confirmed by ^1H NMR spectra of the ligand and complex **1**. The ^1H NMR spectrum of **IQ-1** in DMSO-d_6 displayed a singlet at 13.48 ppm corresponding to the oxime –OH protons. Four doublets and four triplets associated with the aromatic protons of the ligand were observed in the range of 7.67–8.53 ppm [32]. On complexation, the absence of the oxime –OH signal in the ^1H NMR spectra of complex **1** indicated the deprotonation and subsequent coordination of the ligand in an anionic form (Figure S5). The partially overlapping signals associated with the aromatic protons of **IQ-1** in complex **1** appeared within the expected range of 7.60–8.37 ppm with a slight coordination-induced upfield shift. In addition, one sharp singlet of the methyl protons of the Cp* ligand at 1.70 ppm was found in the spectrum of complex **1** with a slight downfield shift relative to the starting $[Ir(Cp^*)Cl_2]_2$ dimer (1.59 ppm). Recording the NMR spectra of complex **2** proved to be impossible due to the negligible solubility of this compound in common deuterated solvents.

2.3. Crystal Structures of the Coordination Compounds

The Ir(III) complex **1** crystallized from the reaction filtrate at 4 °C as red blocks in the centrosymmetric $P2_1/c$ space group, the monoclinic crystal system having a single formula as an asymmetric unit. The structure resembles a typical three-legged piano-stool geometry. The coordination sphere surrounding the Ir(III) center has distorted pseudo-octahedral geometry, provided by the three facial sites from the Cp* ring and three other sites occupied by a chloride anion and two nitrogen atoms of the deprotonated **IQ-1** oxime coordinated in a bidentate chelating fashion (Figure 1). The coordination of **IQ-1** in an anionic form is in accordance with our previously described series of half-sandwich arene-ruthenium(II) complexes [26,27]. The five-membered chelate rings have a bite angle N_2-Ir-N_3 of 78.63(6)°, which is close to the values found in arene-ruthenium(II) complexes with **IQ-1** (78.68–79.47°) [26,27]. The interatomic Ir–N distances involving oxime and heterocyclic nitrogen atoms are 2.1005(14) Å and 2.1534(17) Å, respectively, typical for IrCp* complexes with N,N-ligands [33–35]. The distance between the Ir(III) metal center and the centroid of the Cp* ring is 1.797 Å and the interatomic Ir–Cl distance is about 2.384 Å.

In crystals of true racemate **1**, the heterocyclic oximate ligand **IQ-1** is involved in π–π stacking with an intermolecular distance of 3.342 Å. Moreover, molecules of **1** are involved in CH···Cl short contacts involving the aromatic rings of **IQ-1**: $C_{14}H_{14}\cdots Cl$ ($H_{14}\cdots Cl$ = 2.878 Å, $C_{14}\cdots Cl$ = 3.793 Å, $\angle C_{14}–H_{14}\cdots Cl$ = 162.03°) and $C_{25}H_{25}\cdots O$ short contacts involving the oximate group and the methyl group of Cp* ($H_{25}\cdots O$ = 2.352 Å, $C_{25}\cdots O$ = 3.042 Å, $\angle C_{25}–H_{25}\cdots O$ = 128.85°). These contacts join the identical enantiomers into homochiral chains oriented along the *a* axis (Figure 2).

In the crystal packing of **1**, the homochiral chains are linked by CH···Cl short contacts involving the methyl groups of Cp* ligands, $C_{24}H_{24}$-Cl ($H_{24}\cdots Cl$ = 2.797 Å, $C_{24}\cdots Cl$ = 3.774 Å, $\angle C_{24}–H_{24}\cdots Cl$ = 174.54°) and intermolecular $C_{21}–H_{21}\cdots C_4$ contacts ($H_{21}\cdots C_4$ = 3.077 Å, $C_{21}\cdots C_4$ = 3.766 Å, $\angle C_{21}–H_{21}\cdots C_4$ = 128.57°, Figure 3). The third type of CH···Cl interactions involves the methyl groups of Cp* ligands in the adjacent chains of the same absolute configuration, $C_{21}H_{21}\cdots Cl$ ($H_{21}\cdots Cl$ = 2.657 Å, $C_{21}\cdots Cl$ = 3.629 Å, $\angle C_{21}–H_{21}\cdots Cl$ = 171.31°).

Presumably, these multiply interactions stabilize the centrosymmetric crystal packing and lead to the formation of racemic crystals of **1**.

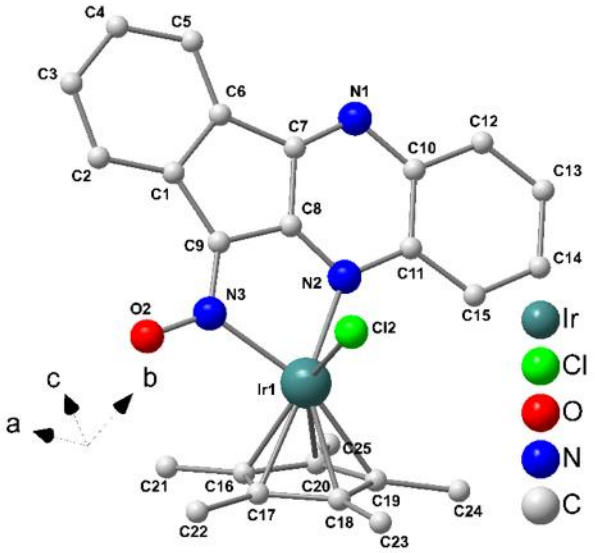

Figure 1. X-ray molecular structure of **1**. Hydrogen atoms are omitted for clarity.

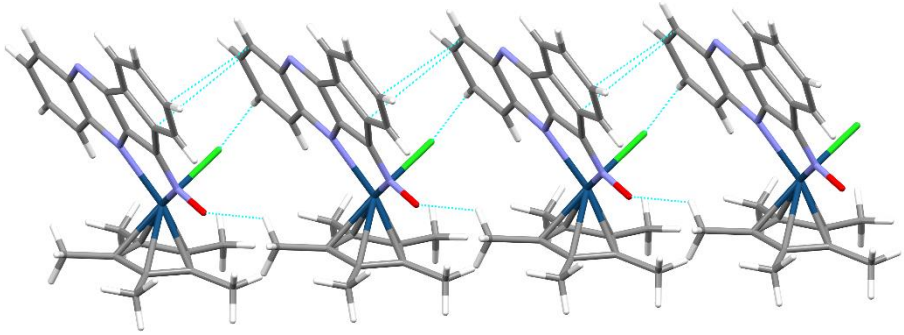

Figure 2. Fragment of the crystal structure of compound **1** showing the homochiral chain oriented along axis *a*. Short contacts are shown as dashed lines.

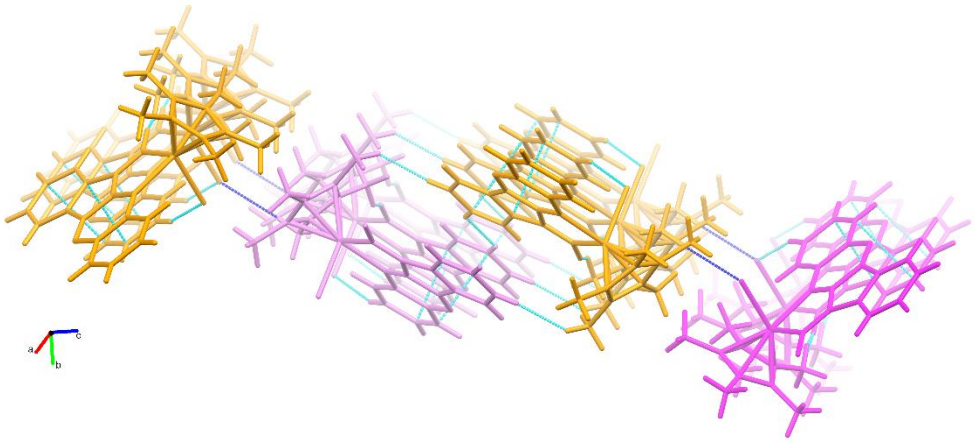

Figure 3. Fragment of the crystal structure of compound **1** showing the supramolecular interactions between the homochiral chains. Short contacts are shown as dashed lines. Enantiomeric chains are colored orange (*R*-) and magenta (*S*-).

In contrast to Ir(III) complex **1**, Rh(III) complex **2** crystallized as fine orange needles in a chiral $P2_12_12_1$ space group forming a racemic conglomerate. Single crystals of the individual enantiomers **2** were selected using the microscope with the polarized lighting (Figure S6). Each isomer from the enantiomeric pair (*S*-**2** and *R*-**2**) was structurally characterized independently with Flack parameters −0.028(15) and −0.015(9), respectively, which are very close to zero within the standard uncertainty, indicative of the correct absolute structure determination (Figure 4). The asymmetric unit in *S*-**2** and *R*-**2** contains one molecule. The coordination arrangement of the Rh(III) metal center is similar to the Ir(III) complex **1** described above.

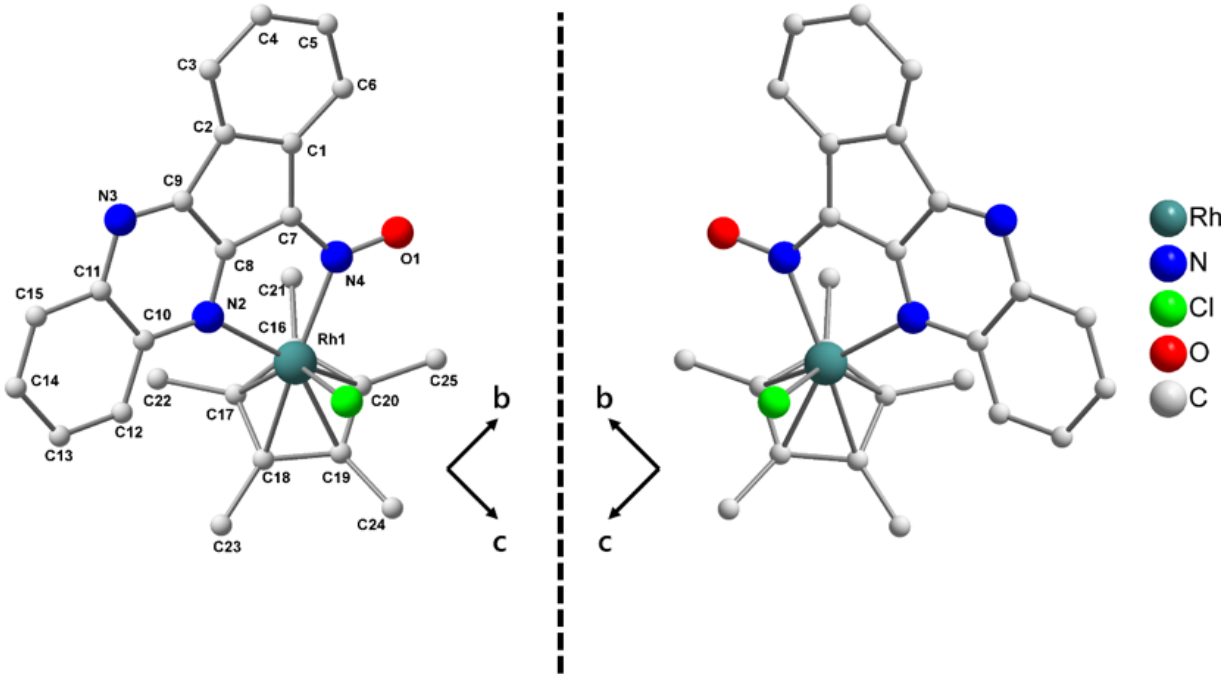

Figure 4. X-ray molecular structures of ***S*-2** (**left**) and ***R*-2** (**right**). Hydrogen atoms are omitted for clarity. Atom numbering is shown only for one of the enantiomers.

The five-membered chelate rings had a bite angle N_1-Rh-N_2 of 79.29° and the interatomic distances Rh–N_2 and Rh-N_1 were 2.160(3) and 2.131(3) Å, respectively, which were somewhat greater than the corresponding distances in Ir(III) complex **1** and RhCp* complexes with N,N′-ligands [36–38]. The interatomic Rh–Cl distance was 2.397(9) Å and Rh–C distances were in the range of 2.137–2.199 Å. The intermolecular interaction pattern in the crystal structure of complex **2** was quite different from the racemic complex **1**. As shown in Figure 5, in the crystal structure of **2** (***S*-** and ***R*-**), the intermolecular CH···C contacts $C_{23}H_{23}\cdots C_5$ ($H_{23}\cdots C_5$ = 2.728 Å, $C_{23}\cdots C_5$ = 3.688 Å, $\angle C_{23}–H_{23}\cdots C_5$ = 166.33°) and $C_{21}H_{21}\cdots C_8$ ($H_{21}\cdots C_8$ = 2.755 Å, $C_{21}\cdots C_8$ = 3.547 Å, $\angle C_{21}–H_{21}\cdots C_8$ = 138.28°) were formed between the methyl groups of Cp* ligand and **IQ-1** aromatic rings. In addition, intramolecular $C_{21}H_{21}\cdots Cl_1$ contacts ($H_{21}\cdots Cl_1$ = 2.879 Å, $C_{21}\cdots Cl_1$ = 3.647 Å, $\angle C_{21}–H_{21}\cdots Cl_1$ = 135.80°) were observed between the methyl groups of Cp* and the chloride ligands. In addition, a combination of intermolecular $C_{23}H_{23}\cdots C_5$ and $C_{13}H_{13}\cdots O_1$ contacts ($H_{13}\cdots O_1$ = 2.826 Å, $C_{13}\cdots O_1$ = 3.089 Å, $\angle C_{13}–H_{13}\cdots O_1$ = 65.27°) led to the formation of a homochiral supramolecular structure. These multiply interactions probably play a key role in the process of the spontaneous resolution of compound **2**.

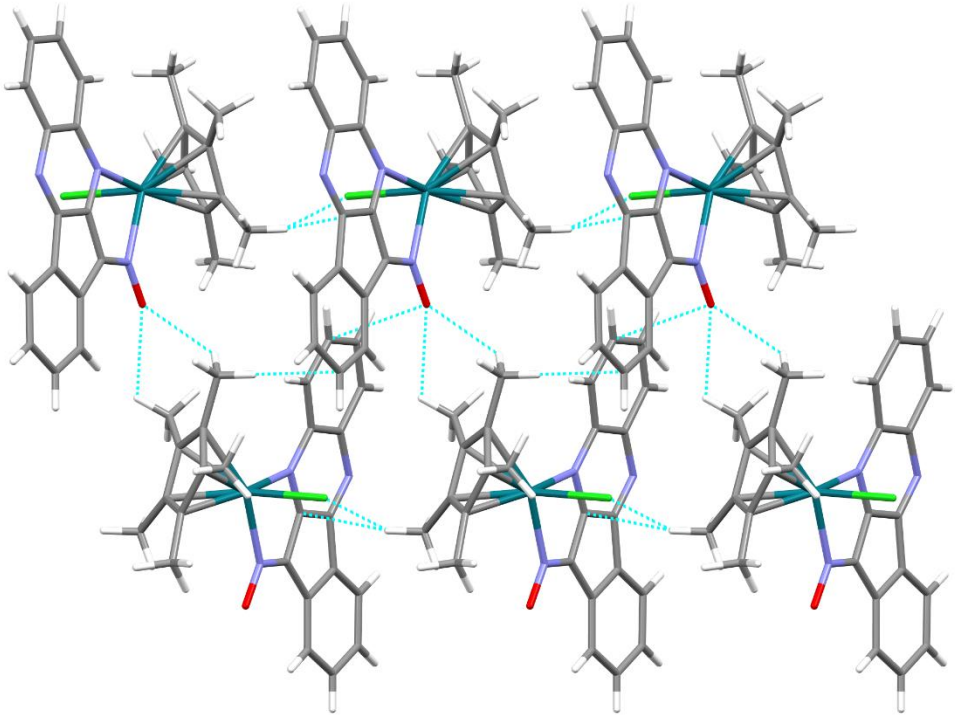

Figure 5. A packing diagram of compound **2** showing a homochiral supramolecular structure (view along axis *c*). Short contacts are shown as dashed lines.

3. Materials and Methods

3.1. Starting Materials and Synthetic Procedures

The dimers $[Ir(Cp^*)Cl_2]_2$ and $[Rh(Cp^*)Cl_2]_2$ were synthesized following the reported procedures [39]. The proligand 11*H*-indeno[1,2-b]quinoxalin-11-one oxime (IQ-1) was prepared as previously described [40].

[Ir(Cp*)(IQ-1)Cl] (**1**). A suspension of $[Ir(Cp^*)Cl_2]_2$ (39,1 mg, 0.05 mmol) in 1 mL of methanol was added to the suspension of **IQ-1** (25 mg, 0.1 mmol) in 1 mL of methanol. The reaction mixture was stirred at room temperature for 24 h. The red powder formed was filtered and washed with methanol to yield 45 mg (74%) of **1**. The filtrate was stored at 4 °C for 12 h to obtain crystals of **1** suitable for X-ray diffraction analysis. NMR ^{1}H (500 MHz, DMSO-d_6): δ = 1.70 (s, 15H, Me-Cp*), 7.61 (t, 1H, L, J = 7.5 Hz), 7.69 (t, 1H, L, J = 7.2 Hz), 7.92 (t, 1H, L, J = 7.0 Hz), 7.95 (d, 1H, L, J = 7.8 Hz), 8.04 (t, 1H, L, J = 7.0 Hz), 8.22 (t, 2H, L, J = 6.5 Hz), 8.36 (d, 1H, L, J = 8.2 Hz) ppm. IR (KBr), cm^{-1}: 3435 w, 2987 w, 2956 w, 2918 w, 1606 m, 1508 s, 1479 s, 1421 s, 1385 m, 1356 s, 1309 s, 1253 s, 1201 s, 1155 m, 1130 m, 1068 m, 1026 m, 968 m, 866 w, 800 m, 765 s, 750 s, 719 m, 619 m, 569 m, 461 m. Found (%): C 49.2, H 3.8, N 6.9; Calculated $C_{25}H_{23}N_3OClIr$ (%): C 49.29, H 3.81, N 6.90.

[RhL(Cp*)Cl] (**2**). A suspension of $[Rh(Cp^*)Cl_2]_2$ (14 mg, 0.022 mmol) in 0.5 mL of methanol was added to a suspension of **IQ-1** (11 mg, 0.044 mmol) in 0.5 mL of methanol. The reaction mixture was stirred at room temperature for 24 h. The bright orange powder that formed was filtered and washed with methanol to yield 12 mg (51%) of **2**. The filtrate was stored at 4 °C for 12 h to obtain crystals of **2** (orange needles) suitable for X-ray diffraction analysis (1.5 mg, 6%). IR (KBr), cm^{-1}: 3145 w, 3028 w, 2802 m, 1641 m, 1604 m, 1577 m, 1510 m, 1490 m, 1466 m, 1427 m, 1340 m, 1325 m, 1307 s, 1203 m, 1155 m, 1124 m, 1063 m, 1001 s, 943 s, 762 s, 735 m, 615 w, 604 w, 590 m, 490 w. Found (%): C 57.6, H 4.3, N 8.5; Calculated $C_{25}H_{23}N_3OClRh$ (%): C 57.76, H 4.46, N 8.08.

3.2. Spectral Methods and Elemental Analysis

Elemental analyses were performed on a Vario MicroCube CHN(S) analyzer (Elementar Analysensysteme GmbH, Langenselbold, Germany). IR spectra were recorded in the

4000 to 400 cm^{-1} region on a Scimitar FTS 2000 Spectrometer (Digilab LLC, Randolph, MA, USA). ^1H NMR spectra were recorded on a Bruker Ascend 500 instrument (Bruker Corporation, Billerica, MA, USA) operating at room temperature (500 MHz for ^1H), and solvent residual peaks were used as internal standards. Powder X-ray diffraction (PXRD) measurements were carried out using a Bruker D8 ADVANCE diffractometer (Bruker Corporation, Billerica, MA, USA), Cu-Kα radiation, λ = 1.5406 Å, 2θ range 3–40°.

3.3. X-Ray Crystal Structure Determination

The single crystal XRD data for **1-2** were collected with a Bruker D8 Venture diffractometer (Bruker Corporation, Billerica, MA, USA) with a CMOS PHOTON III detector and IμS 3.0 source (Mo Kα radiation, λ = 0.71069 Å). All measurements were conducted at 150 K, the φ- and ω-scan techniques were employed. Absorption corrections were applied with the use of the SADABS program [41]. The crystal structures were solved and refined by means of the SHELXT [42] and SHELXL [43] programs using OLEX2 GUI [44]. Atomic thermal displacement parameters for non-hydrogen atoms were refined anisotropically. The positions of hydrogen atoms were calculated corresponding to their geometrical conditions and refined using the riding model. The crystallographic data and details of the structure refinement are summarized in Table 1.

Table 1. Crystallographic data of compounds **1**–**2**.

Compound	**1**	***S*-2**	***R*-2**
Empirical formula	$C_{25}H_{23}N_3OClIr$	$C_{25}H_{23}N_3OClRh$	$C_{25}H_{23}N_3OClRh$
Formula weight	609.15	519.82	519.82
Temperature, K	150(2)	150(2)	150(2)
Crystal system	monoclinic	orthorhombic	orthorhombic
Space group	*P21/c*	$P2_12_12_1$	$P2_12_12_1$
a, Å	8.0606(5)	7.5540(2)	7.5556(2)
b, Å	8.2190(5)	16.0255(4)	16.0214(4)
c, Å	32.182(2)	17.7087(4)	17.7094(4)
α, °	90	90	90
β, °	96.916(2)	90	90
γ, °	90	90	90
Volume, $Å^3$	2116.5(2)	2143.76(9)	2143.75(9)
Z	4	4	4
ρ_{calc}, g/cm^3	1.912	1.611	1.611
μ, mm^{-1}	6.458	0.944	0.944
F(000)	1184	1056	1056
Crystal size, mm^3	0.064 × 0.08 × 0.008	0.12 × 0.03 × 0.03	0.11 × 0.08 × 0.08
2Θ range for data collection, °	5.1176 to 61.1154	3.428 to 61.120	5.085 to 57.3712
Index ranges	$-11 \leq h \leq 11$ $-11 \leq k \leq 11$ $-46 \leq l \leq 45$	$-10 \leq h \leq 10$ $-22 \leq k \leq 22$ $-25 \leq l \leq 25$	$-10 \leq h \leq 10$ $-21 \leq k \leq 21$ $-23 \leq l \leq 23$
Reflections collected	41,035	40,248	38,575
Independent reflections	6502 [R_{int} = 0.0269, R_{sigma} = 0.0168]	6556 [R_{int} = 0.0624, R_{sigma} = 0.0453]	5524 [R_{int} = 0.0386, R_{sigma} = 0.0252]
Restraints/Parameters	0/285	0/285	0/285
Goodness-of-fit on F^2	1.097	1.043	1.045
Final R indices [I >= 2σ (I)]	R_1 = 0.0140, wR_2 = 0.0318	R_1 = 0.0310 wR_2 = 0.0605	R_1 = 0.0174 wR_2 = 0.0392
Final R indices [all data]	R_1 = 0.0153, wR_2 = 0.0322	R_1 = 0.0387, wR_2 = 0.0628	R_1 = 0.0184, wR_2 = 0.0398
Flack parameter	-	−0.028(15)	−0.015(9)
Largest diff. peak/hole, $e \cdot Å^{-3}$	0.699/−0.758	1.236/−0.518	0.271/−0.267

4. Conclusions

The bidentate ligand **IQ-1**, 11*H*-indeno[1,2-b]quinoxalin-11-one oxime formed neutral mononuclear complexes with Ir(III) and Rh(III) ions: [M(L)Cp*Cl]. The Ir(III) complex (**1**) is racemic and crystallizes in a centrosymmetric space group, while the Rh(III) complex (**2**) crystallized in a chiral space group, thus a spontaneous resolution and the formation of a racemic conglomerate from achiral precursors without a chiral additive had taken place. The crystal structures of complexes **1** and **2** (*R*- and *S*-enantiomers) were determined by

X-ray diffraction analysis, and the structural features were compared in order to understand the structural factors, leading to the conglomerate formation. The key difference in the crystal packing of compounds **1** and **2** is the presence of intramolecular interactions (CH···Cl and CH···C) in complex **2**, which bind all three ligands around the chiral metal center. The chiral molecules of 2, stabilized by these intramolecular contacts, are assembled into a homochiral supramolecular network by a combination of intermolecular CH···O and CH···C contacts, leading to the formation of a racemic conglomerate. In the crystal packing of **1**, no specific intramolecular interactions were noted, but multiple intermolecular C–H···C contacts between the chains of enantiomers linked the molecules into the centrosymmetric ensembles and led to the formation of heterochiral crystals of **1**.

Supplementary Materials: The following supporting information can be downloaded at: https://www.mdpi.com/xxx/s1, Figure S1. Experimental and calculated PXRD patterns for complex **1**; Figure S2. Experimental and calculated PXRD patterns for complex **2**; Figure S3. FTIR spectrum of complex **1**; Figure S4. FTIR spectrum of complex **2**; Figure S5. 1H NMR spectrum of complex **1** in DMSO-d6 at 500 MHz; Figure S6. Photograph of the single crystals of compound **2** in the passing polarized light; crystallographic information files (CIF), and checkCIF report files for complexes **1–2**.

Author Contributions: Conceptualization, A.S.P.; Methodology, A.S.P.; Resources, A.S.P.; Investigation, V.V.M. and D.I.P.; Writing—original draft preparation, V.V.M.; Writing—review and editing, A.S.P.; Visualization, D.I.P.; Supervision, A.S.P. All authors have read and agreed to the published version of the manuscript.

Funding: This work was supported by the Ministry of Science and Higher Education of the Russian Federation (Agreement No. 075-15-2022-263). The experiments were performed using large-scale research facilities "EXAFS spectroscopy beamline".

Data Availability Statement: Experimental data associated with this research are available from the authors. Crystallographic data for the structural analysis were deposited with the Cambridge Crystallographic Data Center, CCDC No. 2208391 for compound **1,** 2208389 for compound ***S*-2,** 2208390 for compound ***R*-2**. Copies of the data can be obtained free of charge from the Cambridge Crystallographic Data Center, 12 Union Road, Cambridge CB2 1EZ, UK (fax: +44-1223-336-033; email: deposit@ccdc.cam.ac.uk).

Conflicts of Interest: The authors declare no conflict of interest. The funders had no role in the design of the study; in the collection, analyses, or interpretation of data; in the writing of the manuscript, or in the decision to publish the results.

References

1. Zhang, M.; Zhang, S.-W.; Wu, C.; Li, W.; Wu, Y.; Yang, C.; Meng, Z.; Xu, W.; Tang, M.-C.; Xie, R.; et al. Fine Emission Tuning from Near-Ultraviolet to Saturated Blue with Rationally Designed Carbene-Based [3 + 2 + 1] Iridium(III) Complexes. *ACS Appl. Mater. Interfaces* **2022**, *14*, 1546–1556. [CrossRef] [PubMed]
2. Bi, Y.; Chen, S.; Zhao, H.; Zhang, X. Alkyl-promoted iridium complex for high-performance deep-red phosphorescent organic light-emitting diodes. *Dye. Pigment.* **2022**, *204*, 110484. [CrossRef]
3. Wang, F.; Zhang, L.; Han, W.; Bin, Z.; You, J. Intramolecular C−H Activation as an Easy Toolbox to Synthesize Pyridine-Fused Bipolar Hosts for Blue Organic Light-Emitting Diodes. *Angew. Chem. Int. Ed.* **2022**, *61*, e202205380.
4. Li, H.; Jia, D.; Yao, C.; Jing, Y.; Li, B.; Yang, X.; Sun, Y.; Su, B.; Zhou, G.; Jiao, B. Red-emitting IrIII(CˆN)2(P-donor ligand)Cl-type complexes showing aggregation-induced phosphorescent emission (AIPE) behavior for both red and white OLEDs. *Dye. Pigment.* **2022**, *205*, 110538. [CrossRef]
5. Yoshihara, T.; Matsumura, N.; Tamura, T.; Shiozaki, S.; Tobita, S. Intracellular and Intravascular Oxygen Sensing of Pancreatic Tissues Based on Phosphorescence Lifetime Imaging Microscopy Using Lipophilic and Hydrophilic Iridium(III) Complexes. *ACS Sens.* **2022**, *7*, 545–554. [CrossRef] [PubMed]
6. Wu, S.; Zou, S.; Wang, S.; Li, Z.; Ma, D.-L.; Miao, X. CTnI diagnosis in myocardial infarction using G-quadruplex selective Ir(III) complex as effective electrochemiluminescence probe. *Talanta* **2022**, *248*, 123622. [CrossRef]
7. Ge, Z.-R.; Tong, X.; Huang, Y.-C.; Li, W.-H.; Li, H.-Y.; Lu, A.-D.; Li, T.-Y. Highly Luminescent Dinuclear Iridium(III) Complexes Containing Phenanthroline-Based Neutral Ligands as Chemosensors for Cu^{2+} Ion. *Organometallics* **2022**, *41*, 706–715. [CrossRef]
8. Rashid, A.; Mondal, S.; Mondal, S.; Ghosh, P. A Bis-heteroleptic Imidazolium-bipyridine Functionalized Iridium(III) Complex for Fluorescence Lifetime-based Recognition and Sensing of Phosphates. *Chem.-Asian J.* **2022**, *17*, e202200393. [CrossRef]
9. Štarha, P. Multinuclear biologically active Ru, Rh, Os and Ir arene complexes. *Coord. Chem. Rev.* **2021**, *431*, 213690. [CrossRef]

10. Máliková, K.; Masaryk, L.; Štarha, P. Anticancer Half-Sandwich Rhodium(III) Complexes. *Inorganics* **2021**, *9*, 26. [CrossRef]
11. Pete, S.; Roy, N.; Kar, B.; Paira, P. Construction of homo and heteronuclear Ru(II), Ir(III) and Re(I) complexes for target specific cancer therapy. *Coord. Chem. Rev.* **2022**, *460*, 214462. [CrossRef]
12. Gao, J.; Guo, L.; Wu, Y.; Cheng, Y.; Hu, X.; Liu, J.; Liu, Z. 16-Electron Half-Sandwich Rhodium(III), Iridium(III), and Ruthenium(II) Complexes as Lysosome-Targeted Anticancer Agents. *Organometallics* **2021**, *40*, 3999–4010. [CrossRef]
13. Matton, P.; Huvelle, S.; Haddad, M.; Phansavath, P.; Ratovelomanana-Vidal, V. Recent Progress in Metal-Catalyzed [2+2+2] Cycloaddition Reactions. *Synthesis* **2021**, *54*, 4–32.
14. Kharitonov, V.B.; Muratov, D.V.; Loginov, D.A. Cyclopentadienyl complexes of group 9 metals in the total synthesis of natural products. *Coord. Chem. Rev.* **2022**, *471*, 214744. [CrossRef]
15. Li, P.; Liu, J.-B.; Han, S.; Deng, W.; Yao, Z.-J. Half-sandwich Ir (III) and Rh (III) complexes as catalysts for water oxidation with double-site. *Appl. Organomet. Chem.* **2019**, *33*, e5040. [CrossRef]
16. Burman, J.S.; Harris, R.J.; Farr, C.M.B.; Bacsa, J.; Blakey, S.B. Rh(III) and Ir(III)Cp* Complexes Provide Complementary Regioselectivity Profiles in Intermolecular Allylic C–H Amidation Reactions. *ACS Catal.* **2019**, *9*, 5474–5479. [CrossRef]
17. Yoshino, T.; Satake, S.; Matsunaga, S. Diverse Approaches for Enantioselective C−H Functionalization Reactions Using Group 9 CpxMIII Catalysts. *Chem. Eur. J.* **2020**, *26*, 7346–7357. [CrossRef] [PubMed]
18. Li, M.; Wang, J. Recent Advances on Transition-Metal-Catalyzed Asymmetric C–H Arylation Reactions. *Synthesis* **2021**, *54*, 4734–4752.
19. Liu, C.-X.; Zhang, W.-W.; Yin, S.-Y.; Gu, Q.; You, S.-L. Synthesis of Atropisomers by Transition-Metal-Catalyzed Asymmetric C–H Functionalization Reactions. *J. Am. Chem. Soc.* **2021**, *143*, 14025–14040. [CrossRef]
20. Nielsen, C.D.-T.; Linfoot, J.D.; Williams, A.F.; Spivey, A.C. Recent progress in asymmetric synergistic catalysis—The judicious combination of selected chiral aminocatalysts with achiral metal catalysts. *Org. Biomol. Chem.* **2022**, *20*, 2764–2778. [CrossRef]
21. Bauer, E.B. Chiral-at-metal complexes and their catalytic applications in organic synthesis. *Chem. Soc. Rev.* **2012**, *41*, 3153–3167. [CrossRef] [PubMed]
22. Suzuki, T.; Imamura, T.; Kaizaki, S.; Kashiwabara, K. Preparation, crystal structures and spectroscopic properties of chloro(pentane-2,4-dionato){1,1,1-tris(dimethylphosphinomethyl)ethane}chromium(III), cobalt(III) and rhodium(III) hexafluorophosphate: Comparison of the M-P, M-Cl and M-O (M=Cr, Co and Rh) bo. *Polyhedron* **2002**, *21*, 835–841. [CrossRef]
23. Odinets, I.L.; Artyushin, O.I.; Sharova, E.V.; Goryunov, E.I.; Golovanov, D.G.; Lyssenko, K.A.; Petrovskii, P.V.; Mastryukova, T.A. Generation of an optically active rhodium(III) complex by crystallization-induced spontaneous resolution of a racemic mixture. *Mendeleev Commun.* **2003**, *13*, 102–103. [CrossRef]
24. Gillard, R.D.; Tipping, L.R.H. Optically active co-ordination compounds. Part 39. Resolutions and configurations of compounds containing the cis-bis(ethylenediamine)rhodium(III) moiety. *J. Chem. Soc. Dalt. Trans.* **1977**, 1241–1247. [CrossRef]
25. Schmid, B.; Frieß, S.; Herrera, A.; Linden, A.; Heinemann, F.W.; Locke, H.; Harder, S.; Dorta, R. Chiral amino-phosphine and amido-phosphine complexes of Ir and Mg. Catalytic applications in olefin hydroamination. *Dalton Trans.* **2016**, *45*, 12028–12040. [CrossRef] [PubMed]
26. Matveevskaya, V.V.; Pavlov, D.I.; Sukhikh, T.S.; Gushchin, A.L.; Ivanov, A.Y.; Tennikova, T.B.; Sharoyko, V.V.; Baykov, S.V.; Benassi, E.; Potapov, A.S. Arene-Ruthenium(II) Complexes Containing 11 H-Indeno[1,2- b]quinoxalin-11-one Derivatives and Tryptanthrin-6-oxime: Synthesis, Characterization, Cytotoxicity, and Catalytic Transfer Hydrogenation of Aryl Ketones. *ACS Omega* **2020**, *5*, 11167–11179. [CrossRef]
27. Matveevskaya, V.V.; Pavlov, D.I.; Samsonenko, D.G.; Bonfili, L.; Cuccioloni, M.; Benassi, E.; Pettinari, R.; Potapov, A.S. Arene-ruthenium(II) complexes with tetracyclic oxime derivatives: Synthesis, structure and antiproliferative activity against human breast cancer cells. *Inorg. Chim. Acta* **2022**, *535*, 120879. [CrossRef]
28. Schepetkin, I.A.; Khlebnikov, A.I.; Potapov, A.S.; Kovrizhina, A.R.; Matveevskaya, V.V.; Belyanin, M.L.; Atochin, D.N.; Zanoza, S.O.; Gaidarzhy, N.M.; Lyakhov, S.A.; et al. Synthesis, biological evaluation, and molecular modeling of 11H-indeno[1,2-b]quinoxalin-11-one derivatives and tryptanthrin-6-oxime as c-Jun N-terminal kinase inhibitors. *Eur. J. Med. Chem.* **2019**, *161*, 179–191. [CrossRef]
29. Plotnikov, M.B.; Chernysheva, G.A.; Smolyakova, V.I.; Aliev, O.I.; Trofimova, E.S.; Sherstoboev, E.Y.; Osipenko, A.N.; Khlebnikov, A.I.; Anfinogenova, Y.J.; Schepetkin, I.A.; et al. Neuroprotective Effects of a Novel Inhibitor of c-Jun N-Terminal Kinase in the Rat Model of Transient Focal Cerebral Ischemia. *Cells* **2020**, *9*, 1860. [CrossRef]
30. Liakhov, S.A.; Schepetkin, I.A.; Karpenko, O.S.; Duma, H.I.; Haidarzhy, N.M.; Kirpotina, L.N.; Kovrizhina, A.R.; Khlebnikov, A.I.; Bagryanskaya, I.Y.; Quinn, M.T. Novel c-Jun N-Terminal Kinase (JNK) Inhibitors with an 11H-Indeno[1,2-b]quinoxalin-11-one Scaffold. *Molecules* **2021**, *26*, 5688. [CrossRef]
31. Kovrizhina, A.R.; Samorodova, E.I.; Khlebnikov, A.I. 11H-Indeno[1,2-b]quinoxalin-11-one 2-(4-ethylbenzylidene)hydrazone. *Molbank* **2021**, *2021*, M1299. [CrossRef]
32. Tseng, C.-H.H.; Chen, Y.-R.Y.-L.L.Y.R.; Tzeng, C.-C.C.; Liu, W.; Chou, C.-K.K.; Chiu, C.-C.C.; Chen, Y.-R.Y.-L.L.Y.R. Discovery of indeno[1,2-b]quinoxaline derivatives as potential anticancer agents. *Eur. J. Med. Chem.* **2016**, *108*, 258–273. [CrossRef] [PubMed]
33. Mo, X.-F.; Liu, C.; Chen, Z.-W.; Ma, F.; He, P.; Yi, X.-Y. Metal–Ligand Cooperation in Cp*Ir-Pyridylpyrrole Complexes: Rational Design and Catalytic Activity in Formic Acid Dehydrogenation and CO2 Hydrogenation under Ambient Conditions. *Inorg. Chem.* **2021**, *60*, 16584–16592. [CrossRef] [PubMed]

34. Jordaan, L.; Ndlovu, M.T.; Mkhize, S.; Ngubane, S.; Loots, L.; Duffy, S.; Avery, V.M.; Chellan, P. Investigating the antiplasmodial activity of substituted cyclopentadienyl rhodium and iridium complexes of 2-(2-pyridyl)benzimidazole. *J. Organomet. Chem.* **2022**, *962*, 122273. [CrossRef]
35. Maji, M.; Chakrabarti, K.; Panja, D.; Kundu, S. Sustainable synthesis of N-heterocycles in water using alcohols following the double dehydrogenation strategy. *J. Catal.* **2019**, *373*, 93–102. [CrossRef]
36. Sairem, G.; Anna, V.R.; Wang, P.; Das, B.; Kollipara, M.R. η5 and η6-Cyclic π-perimeter hydrocarbon platinum group metal complexes of 3-(2-pyridyl)pyrazole derived ligands with a pendant nitrile group: Syntheses, spectral and structural studies. *J. Chem. Sci.* **2012**, *124*, 411–419. [CrossRef]
37. Singh, K.S.; Wang, P.; Narkhede, N.A.; Mozharivskyj, Y. Iridium(III) and Rhodium(III) compounds of dipyridyl-N-alkylimine and dipyridyl-NH-ketimine: Spectral characterization and crystal structure. *J. Chem. Sci.* **2017**, *129*, 365–372. [CrossRef]
38. Thangavel, S.; Boopathi, S.; Mahadevaiah, N.; Kolandaivel, P.; Pansuriya, P.B.; Friedrich, H.B. Catalytic oxidation of primary aromatic alcohols using half sandwich Ir(III), Rh(III) and Ru(II) complexes: A practical and theoretical study. *J. Mol. Catal. A Chem.* **2016**, *423*, 160–171. [CrossRef]
39. White, C.; Yates, A.; Maitlis, P.M.; Heinekey, D.M. (η5-Pentamethylcyclopentadienyl)Rhodium and -Iridium Compounds. In *Inorganic Syntheses*; Inorganic Syntheses: Hoboken, NJ, USA, 1992; pp. 228–234. ISBN 9780470132609.
40. Schepetkin, I.A.; Kirpotina, L.N.; Hammaker, D.; Kochetkova, I.; Khlebnikov, A.I.; Lyakhov, S.A.; Firestein, G.S.; Quinn, M.T. Anti-inflammatory effects and joint protection in collagen-induced arthritis after treatment with IQ-1S, a selective c-Jun n-terminal kinase inhibitor. *J. Pharmacol. Exp. Ther.* **2015**, *353*, 505–516. [CrossRef]
41. *APEX2 (Version 2.0), SAINT (Version 8.18c), and SADABS (Version 2.11), Bruker Advanced X-ray Solutions*; Bruker AXS Inc.: Madison, WI, USA, 2012.
42. Sheldrick, G.M. SHELXT—Integrated space-group and crystal-structure determination. *Acta Crystallogr. Sect. A* **2015**, *71*, 3–8. [CrossRef]
43. Sheldrick, G.M. Crystal structure refinement with SHELXL. *Acta Crystallogr. Sect. C* **2015**, *71*, 3–8. [CrossRef] [PubMed]
44. Dolomanov, O.V.; Bourhis, L.J.; Gildea, R.J.; Howard, J.A.K.; Puschmann, H. *OLEX2*: A complete structure solution, refinement and analysis program. *J. Appl. Crystallogr.* **2009**, *42*, 339–341. [CrossRef]